Earth and Planetary Science Letters 287 (2009) 31–42

Contents lists available at ScienceDirect

Earth and Planetary Science Letters

journal homepage: www.elsevier.com/locate/epsl

Size distributions and failure initiation of submarine and subaerial landslides

U.S. ten Brink [a,*], R. Barkan [b], B.D. Andrews [a], J.D. Chaytor [a]

[a] U.S. Geological Survey, Woods Hole Science Center, Woods Hole, MA 02543, USA
[b] Dept. of Geophysics and Planetary Sciences, Tel Aviv University, Tel Aviv, 69978, Israel

ARTICLE INFO

Article history:
Received 19 March 2009
Received in revised form 22 July 2009
Accepted 24 July 2009
Available online 17 September 2009

Editor: R.D. van der Hilst

Keywords:
Inverse Power Law
Lognormal distribution
Continental slope
U.S. East Coast
Ground shaking
Landslides
Slope stability
Northridge earthquake
Self-organized criticality

ABSTRACT

Landslides are often viewed together with other natural hazards, such as earthquakes and fires, as phenomena whose size distribution obeys an inverse power law. Inverse power law distributions are the result of additive avalanche processes, in which the final size cannot be predicted at the onset of the disturbance. Volume and area distributions of submarine landslides along the U.S. Atlantic continental slope follow a lognormal distribution and not an inverse power law. Using Monte Carlo simulations, we generated area distributions of submarine landslides that show a characteristic size and with few smaller and larger areas, which can be described well by a lognormal distribution. To generate these distributions we assumed that the area of slope failure depends on earthquake magnitude, i.e., that failure occurs simultaneously over the area affected by horizontal ground shaking, and does not cascade from nucleating points. Furthermore, the downslope movement of displaced sediments does not entrain significant amounts of additional material. Our simulations fit well the area distribution of landslide sources along the Atlantic continental margin, if we assume that the slope has been subjected to earthquakes of magnitude ≤ 6.3. Regions of submarine landslides, whose area distributions obey inverse power laws, may be controlled by different generation mechanisms, such as the gradual development of fractures in the headwalls of cliffs. The observation of a large number of small subaerial landslides being triggered by a single earthquake is also compatible with the hypothesis that failure occurs simultaneously in many locations within the area affected by ground shaking. Unlike submarine landslides, which are found on large uniformly-dipping slopes, a single large landslide scarp cannot form on land because of the heterogeneous morphology and short slope distances of tectonically-active subaerial regions. However, for a given earthquake magnitude, the total area affected by subaerial landslides is comparable to that calculated by slope stability analysis for submarine landslides. The area distribution of subaerial landslides from a single event may be determined by the size distribution of the morphology of the affected area, not by the initiation process.

© 2009 Elsevier B.V. All rights reserved.

1. Introduction

Submarine slope failures are a major sediment-transport process from the continental shelf and upper slope to the deep ocean (e.g., Hutton and Syvitski, 2004). Slope failure can take different forms such as translational or rotational slides, sediment spreads, debris avalanches, debris flows, and mud flows (Locat, 2001; Locat and Lee, 2002). The different failure forms likely represent the different geotechnical and rheological properties of the failed material, and possible layering and heterogeneity of the site (Locat and Lee, 2002). For example, Harbitz (1992) suggested that a significant part of the Storegga slide failed as a spread. Locat et al. (2009) suggested that the Currituck failure was a retrogressive failure of two separate slides, the deeper one failing first, which caused the adjacent shallower one to fail. As with other retrogressive failures, it is unclear whether these two failures occurred during the same event or were separated in time. The temporal development of slope failure is fundamental to understanding the landslide process, and is also important to the assessment of landslide-generated tsunami, whose runup depends to a large extent on the size of the landslide (e.g., Geist et al., 2009).

In the absence of direct observations, scientists have made assumptions about failure dynamics. The most common assumption is that a landslide process is a cascade or an avalanche process (e.g., Densmore et al., 1998; Guzzetti et al., 2002; Malamud and Turcotte, 2006), known as self-organized criticality (Bak et al., 1988; Hergarten, 2003). This process assumes that failure nucleates in one or more locations, spreads to surrounding regions, and can coalesce to generate large failures. This process is often simulated by cellular-automata models (e.g., Malamud and Turcotte, 2006). The area–frequency distribution of this process is an inverse power law (e.g., Guzzetti et al., 2002).

The avalanche model is by its nature an additive process whose duration can vary widely and cannot be determined at the start of the

* Corresponding author.
E-mail address: utenbrink@usgs.gov (U.S. ten Brink).

0012-821X/$ – see front matter © 2009 Elsevier B.V. All rights reserved.
doi:10.1016/j.epsl.2009.07.031

process (e.g., Turcotte and Malamud, 2004). The most famous example of an additive process in the Earth Sciences is the frequency–magnitude relationship of earthquakes (Gutenberg and Richter, 1944):

$$\log N = a - bM \quad (1)$$

where N is the number of earthquakes with magnitude greater than M occurring over a given time, and a and b are constants. This distribution implies that earthquakes grow from nucleation points and their final magnitude cannot be predicted (e.g., page 274 in Stein and Wysession (2003)). The deviation from power law relationship for small earthquakes is often explained by an incomplete catalog for very small earthquakes, and the deviation at the largest magnitudes is explained by the physical limitation of fault size in different regions (e.g., page 275 in Stein and Wysession (2003)).

An inverse power law distribution was also invoked for different physical aspects of subaerial (Dai and Lee, 2001; Guzzetti et al., 2002; Dussauge et al., 2003; Guthrie et al., 2008; Malamud et al., 2004; Sugai et al., 1994) and submarine (ten Brink et al., 2006a; Micallef et al., 2008) landslides. In the majority of these publications, however, the inverse power law distribution applies only to a truncated portion of the dataset (Stark and Hovius, 2001). To fit the entire range of landslide areas, Malamud et al. (2004) proposed a three-parameter inverse Gamma distribution and Stark and Hovius (2001) proposed a double Pareto function. The misfit of an inverse power law distribution to the portion covering the smallest sizes was attributed to undersampling (e.g., Burroughs and Tebbens, 2001; ten Brink et al., 2006a), to an artifact of the mapping resolution (Stark and Hovius, 2001), or to the transition from a friction-controlled resistance to a cohesion-controlled resistance (Guzzetti et al., 2002).

A few landslide datasets, however, have distributions that are not easily approximated by an inverse power law distribution. Issler et al. (2005) obtained a logarithmic distribution for the volume of depositional lobes from the Storegga slide. Lognormal distributions were found for the areas of landslides in Kashmir (Dunning et al., 2007), and for volumes of deposits of pre-historic turbidity currents in Italy (Talling et al., 2007). Most recently, Chaytor et al. (2009) obtained an excellent lognormal fit to the size distribution of the areas and volumes of 106 submarine slope failure along the Atlantic continental slope ($R^2 = 0.9938$; Figs. 1 and 2). Chaytor et al. (2009) attempted to explain this observation by assuming that the actual size distribution of Atlantic slope failures follows an inverse power law distribution, but that distribution was modified by the conditional probability of preferentially identifying landslides of certain sizes in the bathymetry data to give the appearance of a lognormal distribution.

The portion of the Atlantic continental slope and rise, analyzed here, is a vast area (400,000 km^2), which, with the exception of a 10–20 km-wide upper slope has seafloor slopes $<2°$ (Fig. 1A). Many of the landslides, especially, open slope landslides, initiate on these low-angle slopes (Twichell et al., 2009). The slope of the continental margin could further be characterized as monotonic, i.e., the direction of greatest slope is oriented in the same general direction (seaward) over a large area (Fig. 1B).

In this paper, we show that a simple earthquake-triggered landslide mechanism can produce area distributions that can often be approximated by a lognormal distribution. Although an inverse power law can sometimes approximate the tails of these distributions, we question the physical significance of an inverse power law distribution for landslides. Specifically, we question the assumption that during an event the failure always grows from single or several point-failures and that its final size is unpredictable. (We cannot discard circumstances where the final landslide size may be unpredictable and we briefly discuss one such mechanism at the end of section 4.) The failed material may coalesce into debris flows and turbidity flows as it moves downslope (e.g., Tripsanas et al., 2008), but the downslope movement itself does not excavate significant amounts of new material. Although it is difficult to assess the general validity of this hypothesis, at least one historical record suggests that it could be correct in some cases. Multibeam bathymetry and side-scan sonar surveys of the 1929 Grand Banks landslide, which was triggered by a M7.2 ± 0.3 earthquake, did not reveal evidence for a single major headwall scarp or for a massive slump region (Piper et al., 1999; Mosher and Piper, 2007). Two thirds of the total failure area was characterized by patchy failures with intervening areas showing no evidence of failure. Had the failure been a downslope or upslope cascading process from one or several nucleation points, it is likely that the entire area would have shown evidence for seafloor failure.

The seismological record is also compatible with the hypothesis that failure occurs simultaneously in the area affected by shaking. If landslides nucleate in one location and then propagate along the failure plane similar to earthquake propagation, we would expect large double-couple landslide earthquakes to occur when a large submarine slope failure takes place. Such earthquakes were not detected during the 1929 Grand Banks (Bent, 1995) and the 1998 Papua New Guinea tsunamigenic landslides (Okal and Synolakis, 2001). That said, single-force earthquakes do occur sometime during landslide events (Kanamori and Given, 1982; Okal, 2003). However, these earthquakes are characterized by predominantly long-period surface waves, which are excited by the accelerating and decelerating sliding mass as it interacts with the earth surface during the runout of the debris avalanche (Kanamori and Given, 1982).

We focus here on earthquake-induced landslides from submarine slope failures, and do not discuss other triggering mechanisms (e.g., salt movement, gas hydrate dissociation; Hampton et al., 1996), because triggering of landslides by gas hydrate dissociation has been recently questioned (Hornbach et al., 2007; Twichell et al., 2009), and salt movement is limited to specific locations. Furthermore, examining the statistical characteristics of submarine landslides along the U.S. Atlantic margin, Booth and O'Leary (1991) commented that "the occurrence of large-scale mass movements on gentle slopes implies that regional rather than local factors have been dominant". They further noticed that mass movements along the Atlantic margin tend to be disintegrative and that slope angle does not seem to be an important factor controlling the initiation of a mass movement. These observations suggested to them that a relatively rapid stress increase or strength reduction took place within the sediment column, most likely because of transient earthquake loading (Booth and O'Leary, 1991).

The second part of the paper examines the viability of our hypothesis in the subaerial environment. We suggest that similar to submarine landslides, subaerial landslides also initiate by simultaneous failure over a large area and do not develop as a cascading process. However, the size distribution of these landslides is limited by the morphological characteristics of the failure region.

2. Simulations of earthquake-induced landslides

To test the viability of the hypothesis, we generated Monte Carlo simulations of earthquakes and their expected failure areas and compared their area distribution with the observed distribution along the U.S. Atlantic continental margin (Fig. 2). The maximum expected failure area was estimated using a slope stability analysis with undrained strength properties, following the method and parameters outlined in ten Brink et al. (2009). The method is reviewed here briefly.

Slope failure of sediments is assumed to initiate when the pseudo-static stress, which includes the downslope gravitational stress plus horizontal earthquake loading, exceeds the undrained shear strength. The vertical ground-motion component contains relatively little of the total energy of shaking and is therefore ignored in strong-motion studies (e.g., Harp and Wilson, 1995). This critical pseudo-static stress

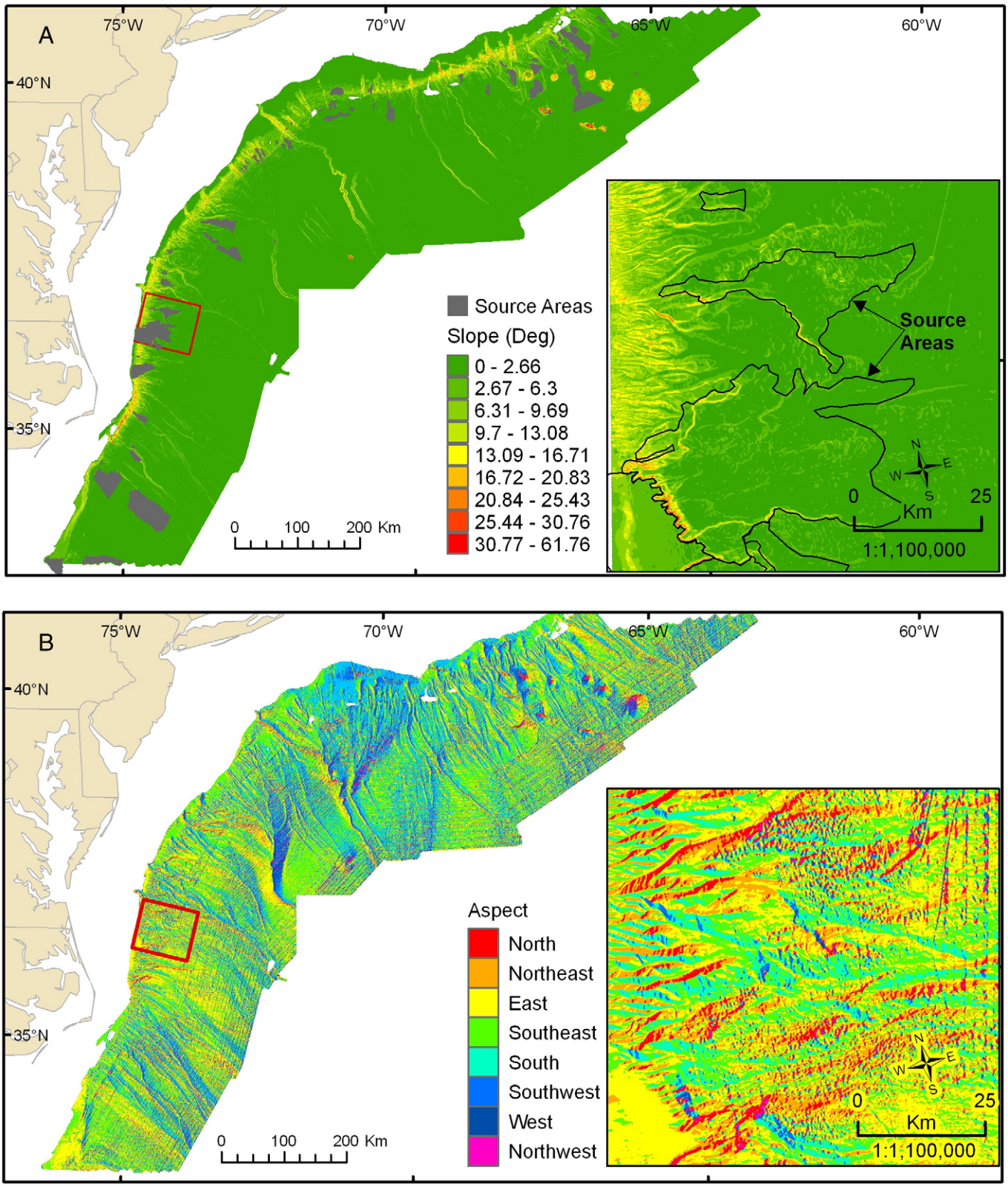

Fig. 1. (A) Slope and (B) aspect maps of the Atlantic continental slope of the U.S., from a bathymetric digital elevation model with a grid-cell resolution of 100 m, derived primarily from compilations of multibeam swath bathymetry (see Twichell et al. (2009) for a full description of the bathymetry data). Landslide source areas (failure scarps) identified by Chaytor et al. (2009), are shown in grey. Aspect is the compass (true) direction of maximum slope and slope is the dip for each 100 m grid cell based on the elevation of its 3×3 cell neighbors. Insets show enlargements of slope and aspect for the continental slope off Chesapeake Bay (red rectangles). The size of the enlarged area is similar to the sizes of areas shown in Fig. 9 to facilitate comparison between submarine and subaerial landslides. Thin parallel lines in (b) are small artifacts in the bathymetry data, which are enhanced by the aspect analysis. (For interpretation of the references to color in this figure legend, the reader is referred to the web version of this article.)

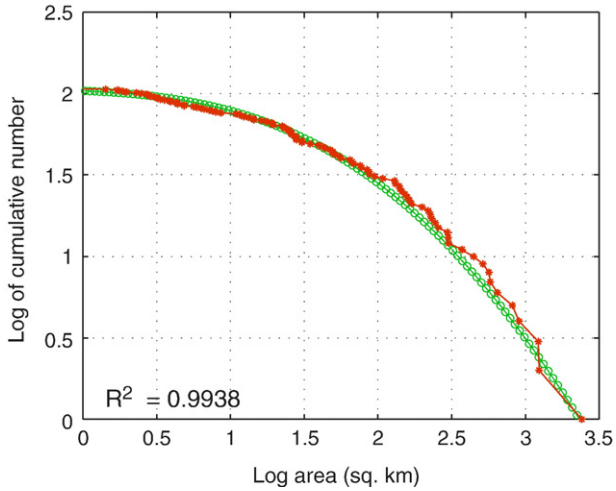

Fig. 2. Observed area distribution of submarine slope failures along the Atlantic continental slope (asterisks), a lognormal fit to the data (circles). Data and fit are displayed as 1-cumulative distribution function (1-CDF).

depends on the slope, sediment density, and the ratio of shear strength to vertical load. However, to cause significant displacement of the material, the peak earthquake acceleration k_{PSA} must exceed sediment shear strength k_y, by a factor of 6.7 or more (Hynes-Griffin and Franklin, 1984; Lee et al., 2000). The peak earthquake acceleration as a function of distance from the rupturing fault, $k_{PSA}(r)$, that we used, is based on empirical and hybrid-empirical attenuation relationships derived from accelerograms and adjusted for the eastern USA (Campbell, 2003). The attenuation relations assume hard rock with shear-wave velocity of 2800 m/s. A site amplification of 3.5 is used (Boore and Joyner, 1997) to account for the measured shear-wave velocity of 300 m/s of shallow sediments on the Atlantic continental slope. A peak spectral acceleration (PSA) at a period of 0.75 s was chosen because the thickness of the sliding layer is typically 20–100 m. (More details about the choice of these and other parameters are provided in ten Brink et al. (2009).) Hence, the *maximum* failure distance from a rupturing fault, r_{max}, is the distance at which the *modified* earthquake acceleration is equal to the sediment shear strength,

$$(3.5 / 6.7) \times k_{PSA} = k_y. \tag{2}$$

The maximum slope failure area A_L can be calculated by using the maximum distance to failure, r_{max}. The maximum failure area is to a first approximation rectangle containing the fault trace, whose length is the fault length L and whose half-width is r_{max}, plus two half circles with radii of r_{max} at either end of the fault as given by

$$A_L = \pi r_{max}^2 + L \times 2r_{max}. \tag{3}$$

Fault rupture length L as a function of earthquake magnitude M is based on the empirical relationship of Wells and Coppersmith (1994) for all faults,

$$L = -2.44 + 0.54M. \tag{4}$$

The calculated area as a function of magnitude is of course a maximum failure area and assumes uniform energy release along the fault. We address in the Discussion cases where the landslide areas are smaller than predicted here. To further simplify the simulations we assume a generic depth profile (Fig. 3), which is qualitatively averaged from 6 depth profiles of the U.S. Atlantic continental margin (Fig. 1), and which represents a several thousand kilometers sector of the margin. The ruptured faults are assumed to be parallel to the shelf edge to reduce the simulations to 2-D. We will account later for deviations of fault orientation from this idealized orientation.

We used the Gutenberg–Richter (G–R) frequency–magnitude distribution (Eq. (1)) to generate the earthquake distribution. The G–R distribution is valid for sufficiently long time intervals and large areas. Observed slope failures along the U.S. Atlantic continental margin and in many passive margins have likely happened over a period of several tens of thousands of years (Lee, 2009). For the U.S. Atlantic margin, we assumed that the U.S. East Coast from 1300 km inland of the shelf edge to 500 km seaward of the shelf edge is a sufficiently large area to follow the G–R earthquake distribution. In the model, the 150-km-wide continental slope begins 150 km seaward of the coast, which mimics the geometry of the U.S. Atlantic margin (Fig. 3).

We placed earthquakes with magnitudes between 4.5 and 7.5 at random locations across this area. The number of earthquakes in each magnitude follows the G–R magnitude distribution. A total of 2348 earthquakes were placed at magnitude intervals of 0.2 to 0.3, assuming that for every one M7.5 earthquake, there are 10 M6.5 earthquakes, 100 M5.5 earthquakes, etc. Magnitudes above 7.5 were not considered because the maximum earthquake magnitude on the U.S. East Coast is assessed to be 7.5 (Frankel et al., 1996; Mazzotti and Adams, 2005). For earthquakes with magnitudes <4.5, the slope stability analysis does not predict the generation of landslides in slopes $\leq 6°$. This prediction is in agreement with observations of earthquake-induced subaerial landslides in the United States, which show that earthquakes with local magnitude $M_L<4$ do not generate landslides, and with inferences suggesting that rock slumps, block slides, rapid soil flows and subaqueous landslides are not generated by earthquake with magnitude $M_L<5$ (Keefer, 1984).

It could be argued that the dissected upper continental slope can give rise to many more small landslides than is considered with our model of a generic slope. An examination of slope dip offshore of Chesapeake Bay, shows that slope dissection by canyons whose walls exceed 6° slope is generally limited to only a ~10 km-wide strip of the slope (inset in Fig. 1). The probability of any of the 1000 M4.5 earthquakes occurring in this 10 km-wide strip of the 1500 km-wide zone of simulation, is 1000 * 10 / 1500 km, or 2 earthquakes will be

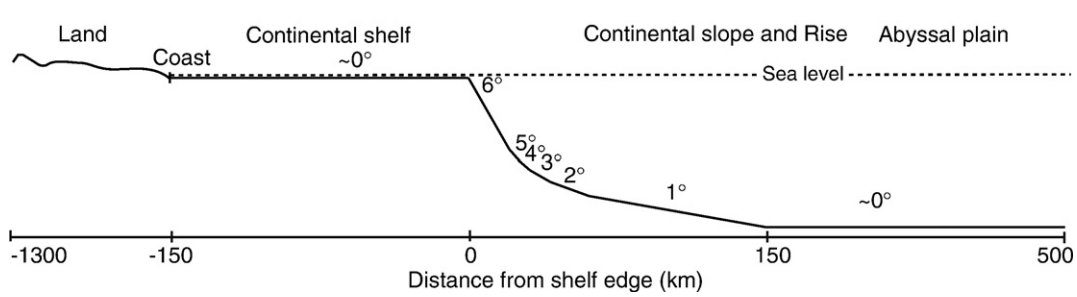

Fig. 3. A generic profile of eastern U.S. and its continental margin, which was used in the calculation of slope stability along the continental slope. Earthquakes were placed at random locations along the profile.

added on average to the simulation results. If M4 earthquakes can generate landslides in slopes that exceed 6°, 4 additional small earthquakes will be added. However, the canyon walls, which are cut into pre-Pleistocene rocks (Pratson et al., 1994), also have a higher strength than was considered in our simulations. The increased wall strength means that the ground shaking amplification is likely to be smaller than the factor of 3.5 used in our simulations (Eq. (2)), and therefore, the peak ground acceleration, k_{PSA}, that is necessary to cause a significant failure should be larger than calculated in our simulations. Therefore, the area distribution of landslides along the Atlantic continental slope will probably not change significantly because small earthquakes cannot generate sufficient ground shaking to cause landslides in these walls.

The maximum failure area for each of the earthquakes was calculated using the slope stability analysis (ten Brink et al., 2009). Earthquakes that are located within the continental slope generate slope failure; those that are far away from the continental slope do not generate slope failures. Those earthquakes that are in the vicinity of the landward and seaward edges of the continental slope generate smaller regions of slope failure in the continental slope. For example, an M7.5 earthquake must be located within 100 km of the continental slope to cause slope failure (ten Brink et al., 2009).

3. Results

The cumulative distribution of the earthquake-induced landslides from these 2348 simulated earthquakes is plotted on a log–log plot (Fig. 4A). Note that only 80 to 150 landslides are generated per simulation, because the majority of the earthquakes are located too far inland to affect the continental slope. Because the location of earthquakes cannot be predicted, the calculation is repeated 1000 times with 1000 different random distributions of earthquake locations. The result (Fig. 4B) shows a consistent cumulative area distribution, with abundant landslides having areas between 10–100 km^2, fewer landslides with area < 3 km^2, and few landslides with areas > 1800 km^2 (Fig. 4C). The 1000 modeled landslide distributions fit well a lognormal distribution ($R^2 > 0.97$). Hence, the paucity of small landslides relative to the number predicted by an inverse power law relationship may not be due to undersampling, but instead due to the fact that small magnitude earthquakes cannot generate landslides unless the seafloor slope is very steep, whereas the areal extent of seafloor with steep slopes is small. Although some (but not all) of the realizations show a relatively linear tail of cumulative area distribution, the curve does not have a distinct slope break that would allow a certain range of the population to be fit by an inverse power law curve.

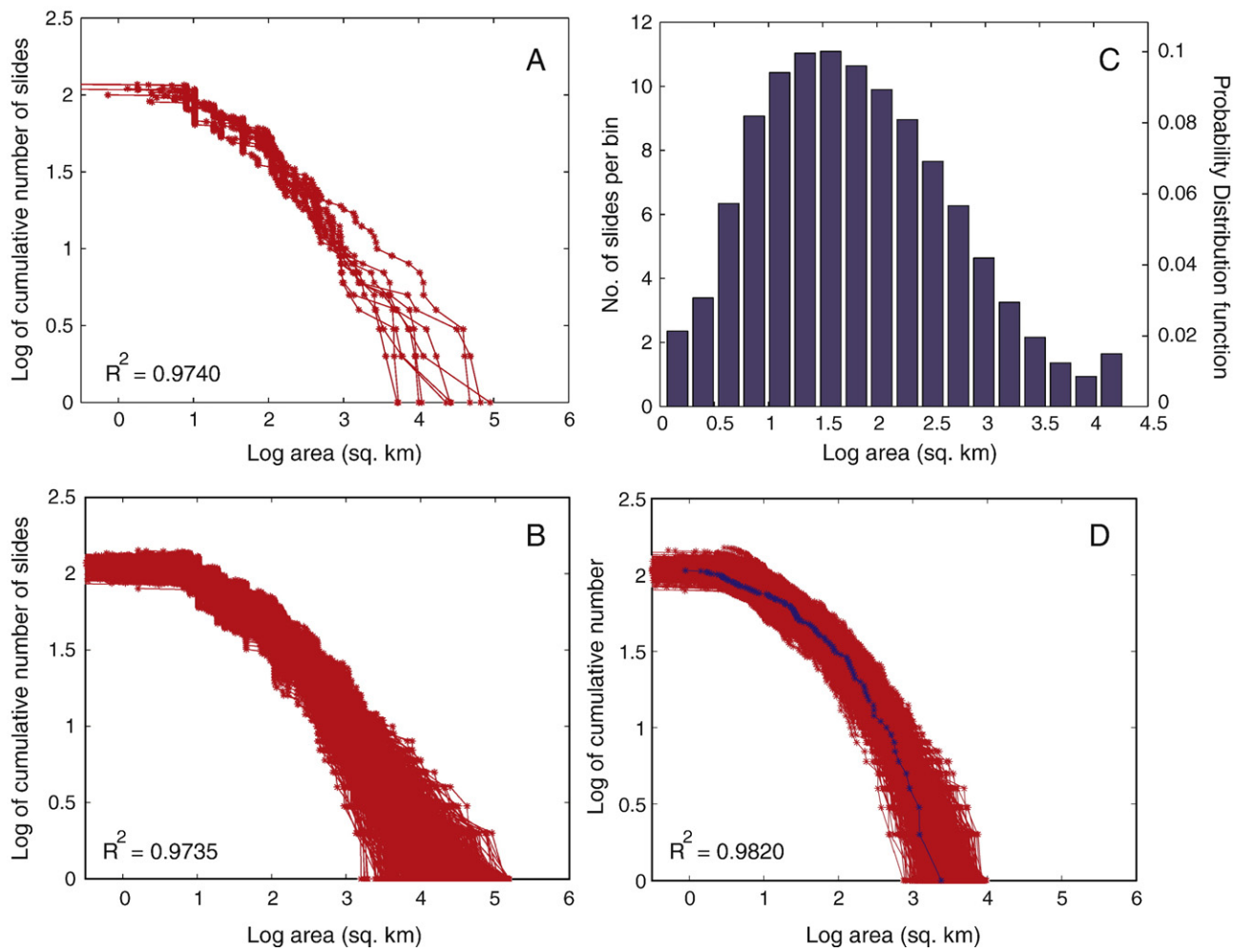

Fig. 4. (A) 10 and (B) 1000 predicted area curves calculated using the relationship between slope stability and earthquake magnitude, and the Gutenberg–Richter distribution of earthquake magnitudes. The small steps in the curves are caused by using earthquake magnitude increments of 0.2 to 0.3, in the area calculation. Curves are displayed as 1-CDF. The average of the squares of the correlation coefficients of each curve with a lognormal distribution, R^2, is shown. (C) Probability Distribution Function (PDF) of the area distribution curves in (B). The shown PDF is the mean of all 1000 PDFs. PDFs were calculated by binning the range of areas on a logarithmic scale. (D) Same as (B), except that the range of earthquake magnitudes is limited to between 4.5 and 6.3, instead of 4.5 and 7.5. The predicted failure area is multiplied by a random number between 0.3–1 to account for the fact that only part of the maximum predicted area may fail during an earthquake. Note the good fit with the observed area distribution of submarine slope failures along the Atlantic continental slope (blue curve). (For interpretation of the references to color in this figure legend, the reader is referred to the web version of this article.)

Thus we show that given the assumption that the area of slope instability is a function of the magnitude of ground shaking, and given a G–R frequency–magnitude distribution of earthquakes, the expected cumulative distribution of landslide areas does not follow an inverse power law, but may in fact be closer to a lognormal distribution. Lognormal distribution appears to fit both the data and the simulations better than an inverse gamma distribution (Fig. 5). An inverse power law fit to the portion of the data that includes only the largest 49 slides (log area > 1.5) is also inferior to a lognormal fit (Fig. 5). However, we do not imply a genetic significance to lognormal distribution, but only that it represents a situation in which landslides have a characteristic area and the number of landslides falls off with both decreasing and increasing sizes.

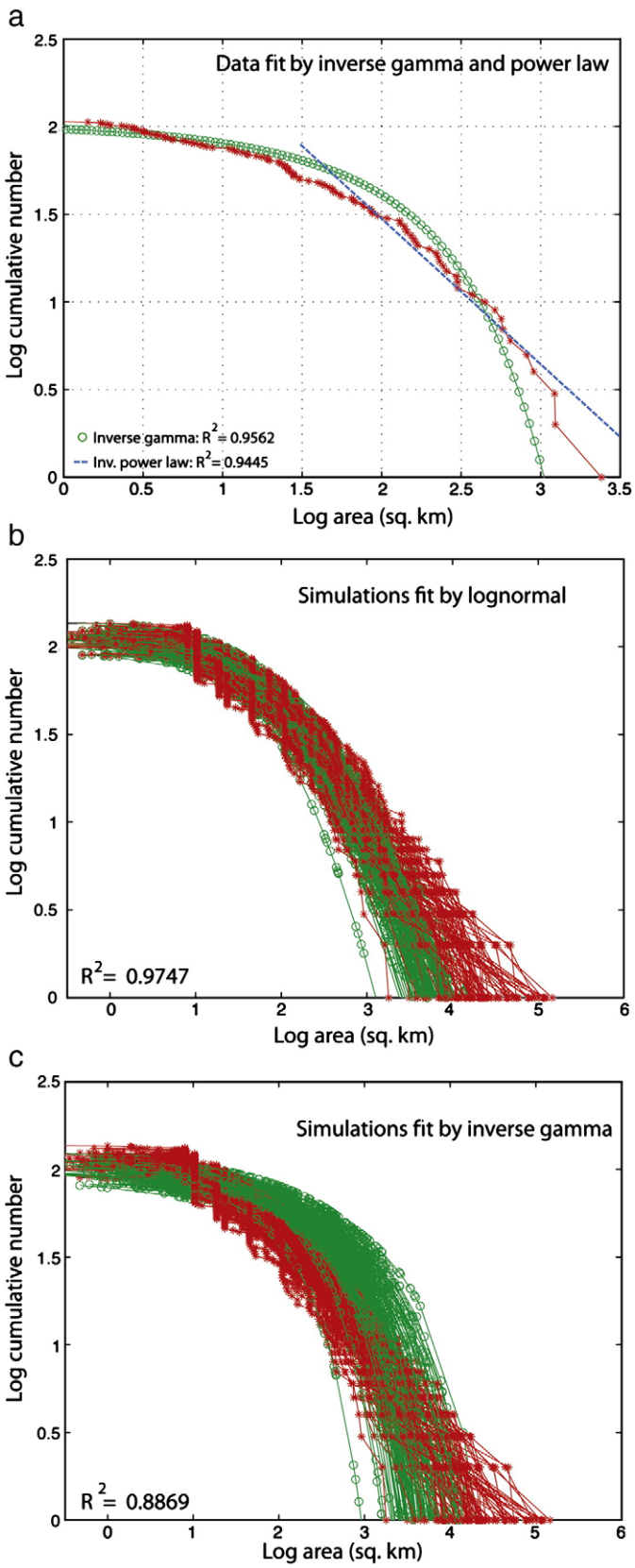

Fig. 5. (a) Observed area distribution of submarine slope failures along the Atlantic continental slope (red asterisks) and a two-parameter inverse gamma fit to the data (green circles), and an inverse power law fit to a truncated portion (areas > log1.5) of the data (blue dashed line). (b, c) 100 predicted area distribution curves (red) calculated using the relationship between slope stability and earthquake magnitude, and the G–R distribution of earthquake magnitude and their corresponding (b) lognormal and (c) inverse gamma curve fits (green circles). The R^2 value is the average of the squares of the correlation coefficients for each curve. 100 curves are shown instead of 1000 curves for clarity. The calculated curves are for the range of earthquake magnitudes between 4.5 and 7.5, an 1800 km-wide area, and a maximum failure area for each earthquake magnitude. Curves are displayed as 1-CDF, where CDF is the cumulative distribution function.

4. Discussion

Earthquake distributions in different regions have different maximum magnitudes depending on geological conditions and fault types in these areas (e.g., Stein and Wysession, 2003). We investigated the possibility of a smaller maximum earthquake magnitude in this continental margin by limiting the G–R frequency–magnitude to a range between M4.5 and M6.3. This range does not imply that larger magnitude (M6.4–M7.5) earthquakes cannot occur on land simply that larger earthquakes located more than 100 km landward from the shelf edge are not expected to cause failures on the continental slope (ten Brink et al., 2009). Therefore, such larger earthquakes on land will not have an effect on this simulation. The limited range of earthquake magnitudes has a significant effect on the shape of the area distribution. The largest expected failure areas are much smaller (by an order of magnitude) than those predicted with a wider magnitude range (M4.5–M7.5), and the area distribution continues to curve and has no flat tail (compare Fig. 4D to 4B). In other words, the effect of a narrow range of earthquake magnitudes is to trim the outer tail.

Simulations with a limited earthquake magnitude range (M4.5–M6.3) show a good fit to the area distribution of 106 landslides along the Atlantic continental slope (Fig. 4D). The observed good fit suggests an interesting possibility; the shape of the observed area distribution of submarine landslides may be indicative of the range of earthquake magnitudes in that area. Similar studies in other regions are needed to verify this suggestion.

The size of the region in which the G–R magnitude–frequency distribution applies is not well defined (see discussion in Stein and Wysession (2003)). To test the effect of the assumed total area, we calculated our simulations with the total area extending only 400 km inland from the coast (Fig. 6b), instead of 1300 km (Fig. 6a). In other words, the probability for earthquakes to be located within or close to the continental slope was doubled (150/900 = 16.6% instead of 150/1800 = 8.3%). Although a larger number of landslides (180–250 vs. 80–150) were predicted, the shape of the curve and its fit to the lognormal area distribution remained the same.

The failure area calculated by the slope stability analysis is a maximum area. It is likely that the fault does not have a uniform energy release, and only part of the area fails during an earthquake, the rheology and pore pressure are not spatially uniform, or the fault orientation is not parallel to the strike of the margin, as in our simplified simulations. To mimic these situations, we decreased the predicted failure area by multiplying each failure area from each

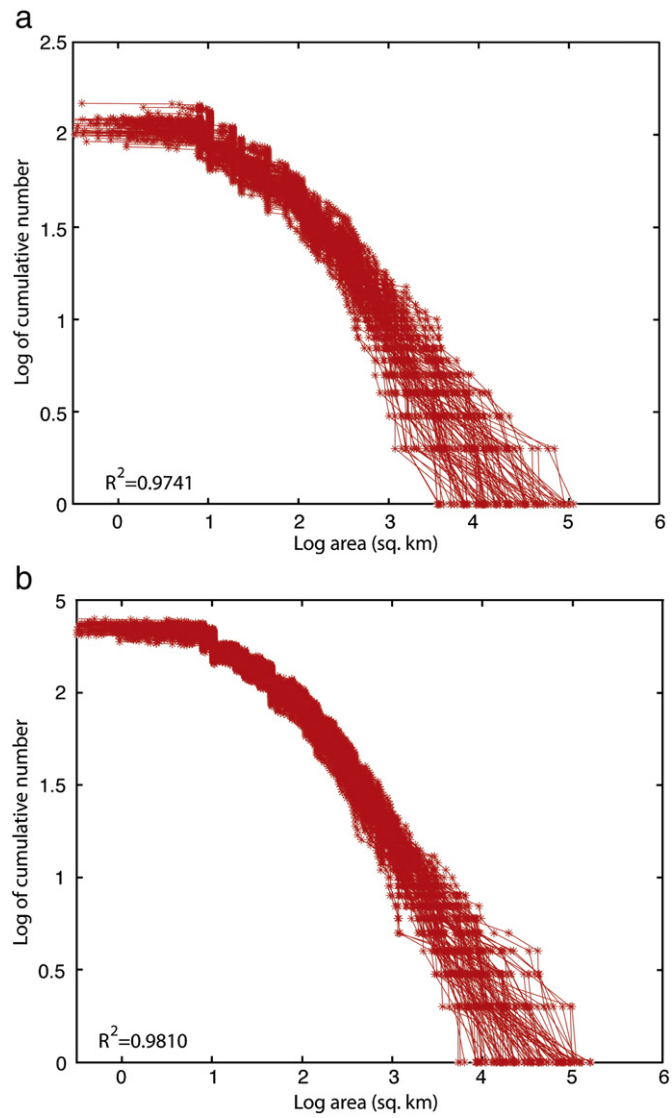

Fig. 6. (a) 100 predicted area distribution curves calculated using the relationship between slope stability and earthquake magnitude, and the G–R distribution of earthquake magnitude. It is similar to Fig. 4, but for clarity shows 100 curves, instead of 1000 curves. The R^2 value is the average of the squares of correlation coefficients for each curve. The calculated curves for an 1800 km-wide area, earthquake magnitudes between 4.5 and 7.5, and a maximum failure area for each earthquake magnitude. (b) Same as (a) but for a 900 km-wide area.

earthquake by a random factor ≤ 1. In the absence of information about the probability distribution of this factor, we assumed, for example, a range of 0.3–1 for this factor, with all values between 0.3 and 1 having an equal probability. The contribution of this multiplier to the shape of the distribution is small (Fig. 7a), therefore, the simulations cannot help us determine how often the maximum predicted area fails vs. part of the area. Simulations with multipliers ranging between 0.6–1 and 0.1–1 were also tested and gave similar results. However, the observed landslide distribution along the U.S. Atlantic margin is plotted at the center of the 1000 simulated curves that were generated with a multiplier range between 0.3–1 (Fig. 4D), whereas it has smaller areas relative to most curves generated by simulations where the maximum area is always expected to fail (multiplier of 1; Fig. 8). The comparison to observations therefore, suggests that slope failures generally do not reach their maximum calculated area, as was expected intuitively.

The relationship between slope stability analysis and earthquake magnitude depends on many parameters, some of which are empirical (ten Brink et al., 2009). To account for potential variations in that relationship, we multiplied each failure area by a random factor between 1 and 2 (Fig. 7b). As expected, the predicted areas are slightly larger, but the overall shape of the curves is similar to that in Fig. 6a and it can still be fit quite well by lognormal distribution.

Translational slides of relatively non-cohesive material, such as along the U.S. Atlantic margin, may undergo simultaneous slope failure over a large area during ground shaking. However, other submarine landslides may still obey an inverse power law. For example, the inverse power law distribution of areas and volumes of submarine landslides north of Puerto Rico (ten Brink et al., 2006a) may be controlled by the distribution of fractures, and not by earthquake magnitude. These mostly rotational landslides erode the edge of a massive, tilted carbonate platform. Fissures and fractures observed in multibeam bathymetry images at the edge of the platform (ten Brink et al., 2006b) probably develop by tensile stresses and grow by carbonate dissolution in a system of seawater circulation. Slope failures during earthquakes may follow these fractures. Tensile fracture systems (Katz and Aharonov, 2006) and faults (Scholz and Cowie, 1990) have been shown to obey an inverse power law distribution in the lab and in the field, attesting to their progressive development.

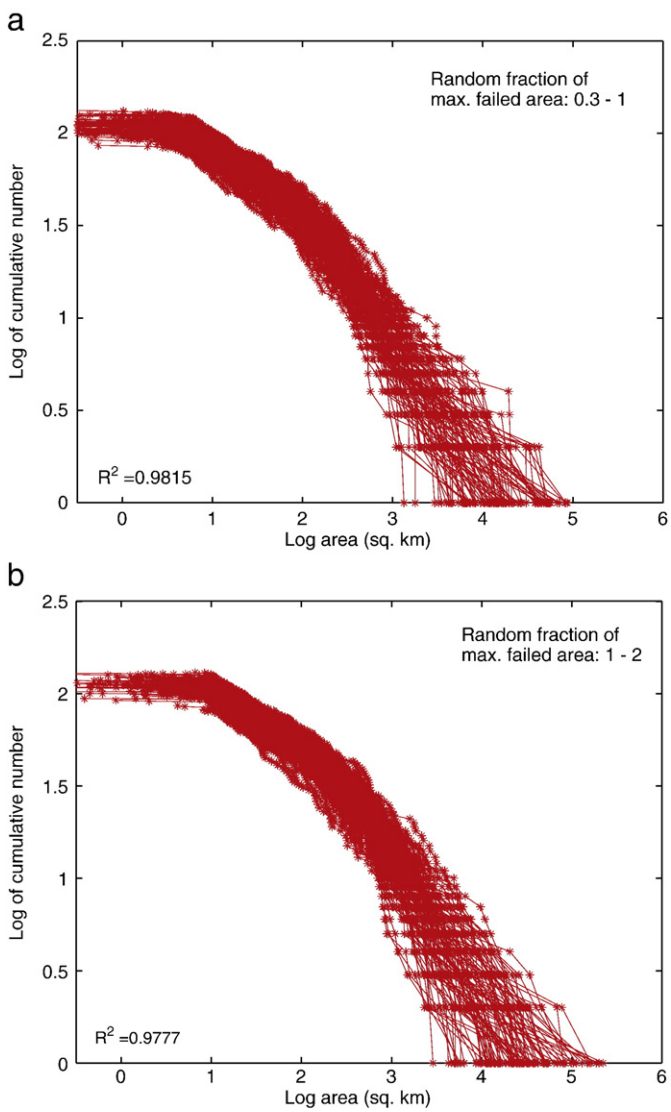

Fig. 7. (a) Same as Fig. 6a), but when only part of the failure area predicted from the slope stability-earthquake magnitude relationship, fails. The fraction of the failed area varies randomly between 0.3 and 1. (b) Same as (a), except that the failed area can be up to twice that of the calculated maximum failure area; i.e., the predicted failure area is randomly multiplied by a factor ranging between 1 and 2. Despite the seemingly linear tail, the curves can be fit well by lognormal distribution as shown by the R^2 value.

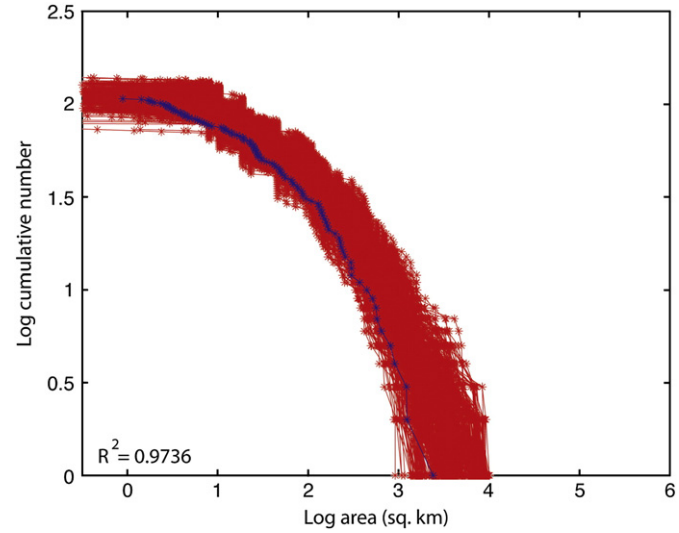

Fig. 8. Same as Fig. 4D, except that the maximum predicted failure is always assumed to fail. Note that most of the simulations over-predict the observed area distribution of submarine slope failures along the Atlantic continental slope (blue curve). (For interpretation of the references to color in this figure legend, the reader is referred to the web version of this article.)

5. Subaerial vs. submarine landslide distribution: the role of morphology

As mentioned in the Introduction, area–number distribution of subaerial landslides was shown to fit inverse power law distribution (e.g., Dai and Lee, 2001), three-parameter Gamma distribution (Malamud et al., 2004), and double Pareto distribution (Stark and Hovius, 2001). In this section we attempt to reconcile these observations with the distribution of submarine landslides along the U.S. Atlantic margin. We propose that the total area which encompasses earthquake-triggered subaerial landslides is similar to that predicted for submarine landslides, but the distribution of subaerial landslides is shaped by the morphological characteristics of the area. We used similar grid size (100 × 100 m) and similar size area (80 × 90 km) when comparing the morphological characteristics of subaerial and submarine landslide regions.

More than 11,000 small ($10^{-5} - 2 \times 10^{-1}$ km^2) landslides were generated within a total area of 10,000 km^2 as a result of the M6.7 1994 Northridge earthquake in southern California (Harp and Jibson, 1995). The landslide areas are several orders of magnitude smaller than submarine landslides along the Atlantic continental slope (Fig. 2). This area of southern California is generally characterized by high slope angles (> 13° in many parts, Fig. 9A), much higher than the U.S. East Coast. The difference in the direction of greatest slope (also known as 'aspect') is even more striking. In the Northridge area, the direction is almost evenly distributed in all compass directions with each of the 8 principal directions covering at least 10% of the total area (Figs. 9A and 10A). The slope directions vary over short distances as can be seen by the fact that the average aspect polygon is only 0.05–0.075 km^2, and does not show preference to a particular compass direction (Fig. 10B). (An aspect polygon is the area of one or more contiguous cells with the same slope direction.) Contrast these characteristics with a subset area of the continental slope off of Chesapeake Bay (insets in Fig. 1), which is heavily dissected by submarine canyons, and which has the same area and grid resolution (100 × 100 m) as the Northridge area. The vast majority (87%) of slope directions in that area are between NE and S (45°–180°) (Fig. 10A). Furthermore, aspect polygons with slope directions between NE and S are on average quite large (up to 0.382 km^2) with a maximum of 246 km^2 (Fig. 10B). The morphological characteristics of the Atlantic continental slope and rise were shaped by sediment progradation over a very long geological time period coupled with along-slope current deposition and erosion and minor shelf edge erosion during sea level minima. In particular, the morphology of the slope and rise has been modified by high rate of sediment accumulation and transport, often covering pre-existing canyons and slide scarps (Pratson et al., 1994). The morphology of the Northridge area, in contrast, is progressively dissected by subaerial erosion and tectonic uplift.

Fig. 9. Slope (A, C and E) and aspect maps (B, D and F) for three areas of subaerial landslides, Northridge, CA, Umbria, Italy, and southern Guatemala. Landslides in the Northridge area were triggered by the 1994 M6.7 earthquake (Harp and Jibson, 1995), in the Umbria area by a heavy snowfall in 1997 (Guzzetti et al., 2002), and in Guatemala, by rain from hurricane Mitch in 1999 (Bucknam et al., 2001). Elevation data sources are: Northridge — http://seamless.usgs.gov/index.php resampled from 30 to 100 m; Umbria — two SRTM tiles http://edcsns17.cr.usgs.gov/EarthExplorer with 100 m a grid cell that covers most of the Umbria landslides discussed in Guzzetti et al. (2002); Guatemala — scanned 1:50,000 topographic maps, Rio Hondo and Pueblo Viejo sheets, resampled from 10 m cell resolution to 100 m with background shaded relief from SRTM. All scales and cell resolutions are identical and are also similar to those in the insets of Fig. 1 to facilitate comparison.

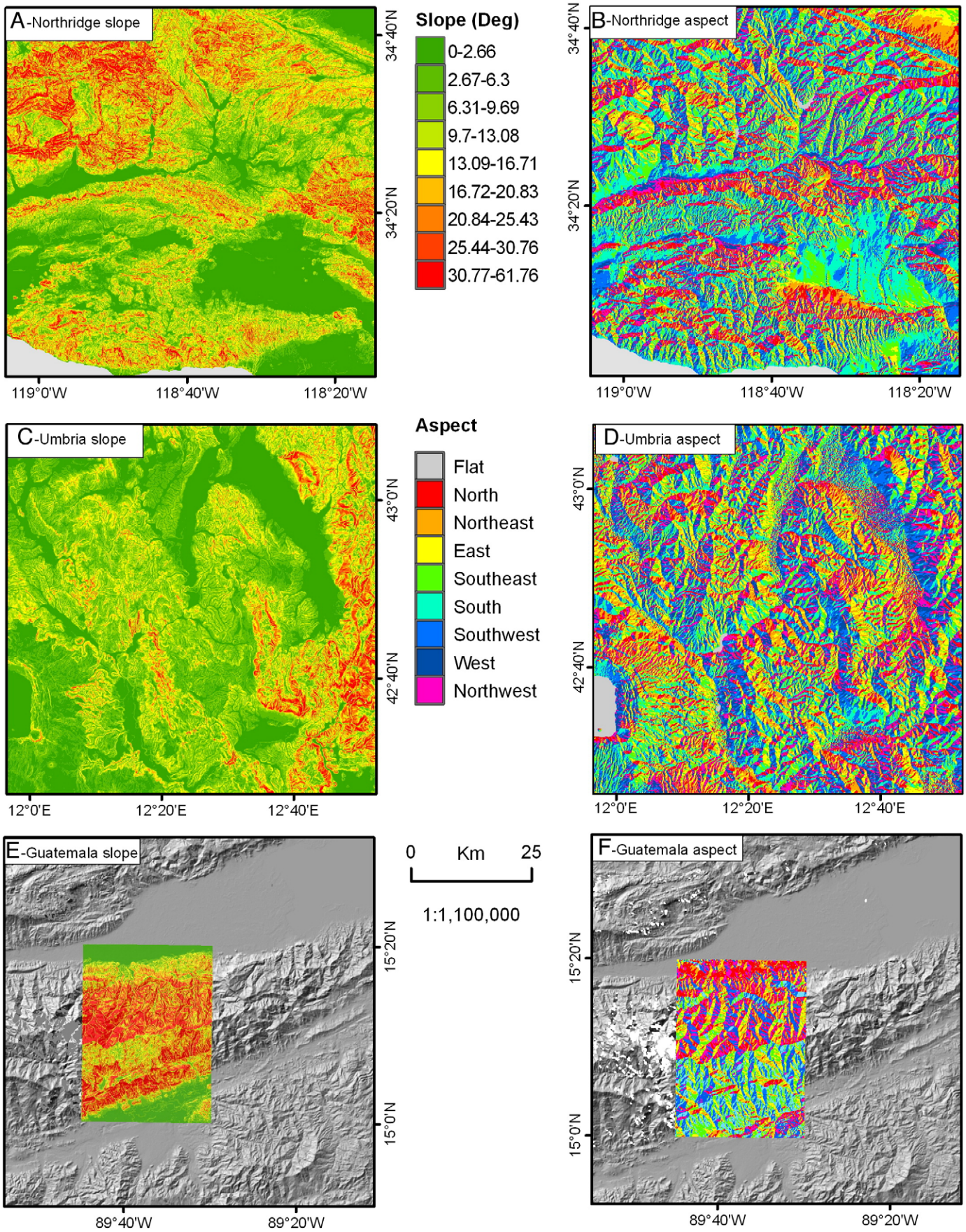
A-Northridge slope
B-Northridge aspect
C-Umbria slope
D-Umbria aspect
E-Guatemala slope
F-Guatemala aspect
Slope (Deg)
0-2.66
2.67-6.3
6.31-9.69
9.7-13.08
13.09-16.71
16.72-20.83
20.84-25.43
25.44-30.76
30.77-61.76
Aspect
Flat
North
Northeast
East
Southeast
South
Southwest
West
Northwest
0 Km 25
1:1,100,000
34°40'N
34°20'N
119°0'W
118°40'W
118°20'W
43°0'N
42°40'N
12°0'E
12°20'E
12°40'E
15°20'N
15°0'N
89°40'W
89°20'W

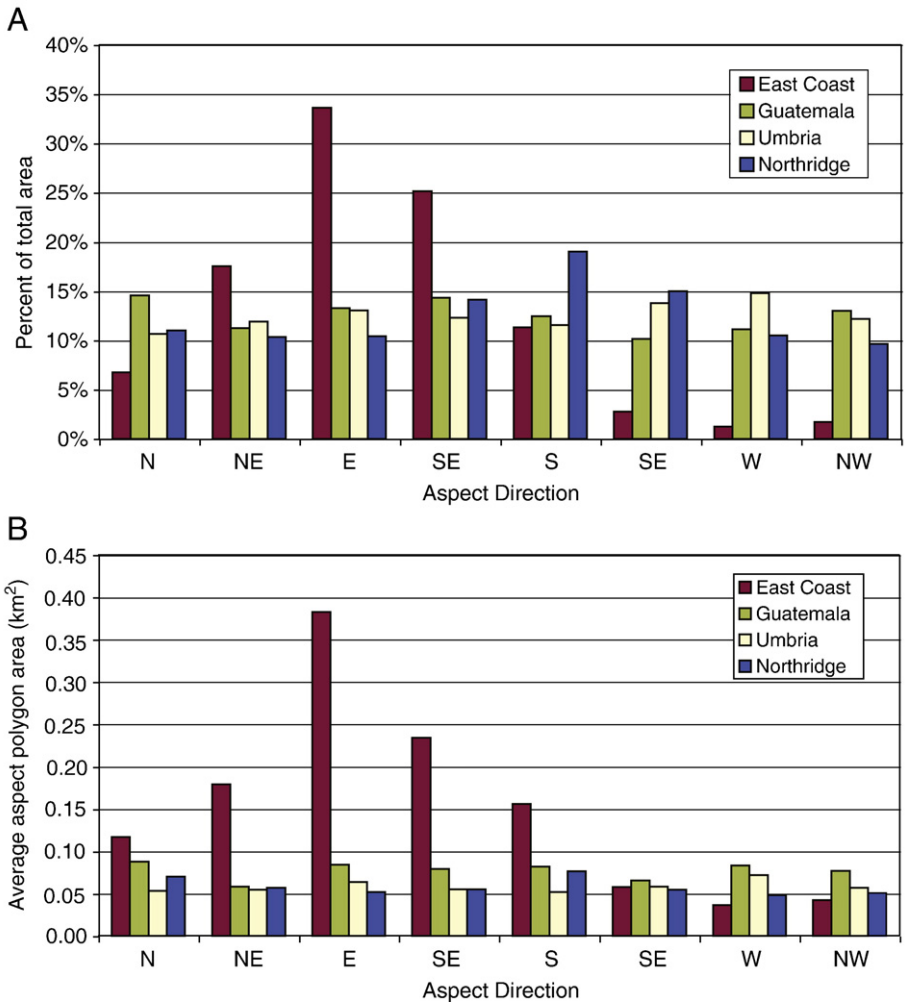

Fig. 10. Statistical summaries of the aspect maps shown in Fig. 1B-inset and Fig. 9. (A) Total area of polygons with similar compass direction as a percentage of the total map area. Note that the three land areas have roughly equal portion of the total area (10–15%) in each compass direction, whereas 87% of the continental slope area in Fig. 1-inset is in directions between NE and S. (B) Average area (in km^2) of aspect polygons in each compass direction. (Aspect polygon is one or more contiguous cells with the same dip direction.) Note that the three land areas have roughly equal average area of 0.05–0.075 km^2 in all directions, whereas the continental slope has much larger average areas in the dominant slope directions.

Despite the differences in morphological character between the submarine and subaerial environments, the observed maximum total area affected by subaerial landslides as a function of earthquake magnitude on land (Keefer 1984; Rodriguez et al., 1999) is comparable in size with that calculated for the Atlantic continental slope from slope stability analysis, (Fig. 11, ten Brink et al., 2009). Each submarine landslide can be considered, based on this comparison, as a composite of many small landslides of variable sizes, similar to observations on land, with the only differences being that submarine slopes generally trend seaward and are less variable in dip angle. The lack of continuous failure features within the 1929 Grand Banks landslide, discussed earlier, is compatible with this view.

The published power law, Gamma, and double Pareto distributions of subaerial landslides may be functions of morphological constraints on the area of landslides, not the underlying landslide driving force. For example, the truncated area distribution of landslides triggered by the 1994 Northridge earthquake follows an inverse power law (Malamud et al., 2004; Fig. 12). Notably, the cumulative area distribution of aspect polygons in the topography of the Northridge area also follows an inverse power law with a slope of 1.6 similar to the distribution of landslide areas (Fig. 12). Other effects on the area distribution of landslides in some places may include variations in soil moisture contents (Pelletier et al., 1997), the presence of shallow fault planes, topographic site effects (Meunier et al., 2008), and slope and lithology changes (Jibson et al., 1998).

Malamud et al. (2004) were able to fit inverse gamma distribution with similar parameters to three landslide populations resulting from 3 different triggering events: the 1994 Northridge earthquake, the 1998 Hurricane Mitch-related rainfall in Guatemala, and the rapid snow melt in Umbria (Italy) in 1997. The fit to all 3 populations may be explained by the limitation on failure area imposed by the available slope area. These 3 areas are located in tectonically-active mountainous regions and share similar morphological characteristics. All 3 areas are characterized by very high slope angles (Fig. 9). The slope directions are distributed equally around all compass directions (Figs. 9 and 10A) and the average size of each aspect polygon is 0.05–0.08 km^2 regardless of compass direction (Fig. 10). These statistics express the morphology of mountainous regions being composed of many small areas with a wide range of slope directions (Fig. 9B, D, and F). Therefore, we suggest that when a failure is triggered in such areas by any mechanism, it is characterized by many separate small slides, and the maximum size of each landslide is limited by the morphology.

6. Conclusions

We use the area distribution of submarine landslides along the Atlantic continental slope of the U.S. and other supporting evidence to

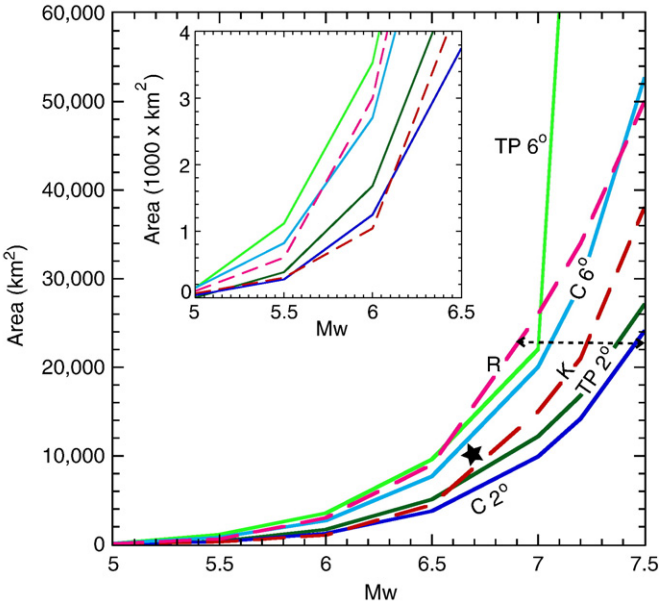

Fig. 11. Comparison between two methods to derive the relationship between earthquakes and landslide areas. Solid curves were calculated by the slope stability analysis method for seabed slopes of 2° and 6° with the peak spectral acceleration (PSA) relationships for the eastern U.S. of Campbell (2003) (C2° and C6°) and Tavakoli and Pezeshk (2005) (TP2° and TP6°). Dashed curves are empirical relationships of maximum failure area on land, K (Keefer, 1984) and R (Rodriguez et al., 1999). Inset — Enlargement for low earthquake magnitudes. Star — Total area affected by landslides due to the M6.7 Northridge earthquake (Harp and Jibson, 1995). Double-arrowed dashed line - total area affected by landslides from the M7.2±0.3 Grand Banks earthquake (Mosher and Piper, 2007).

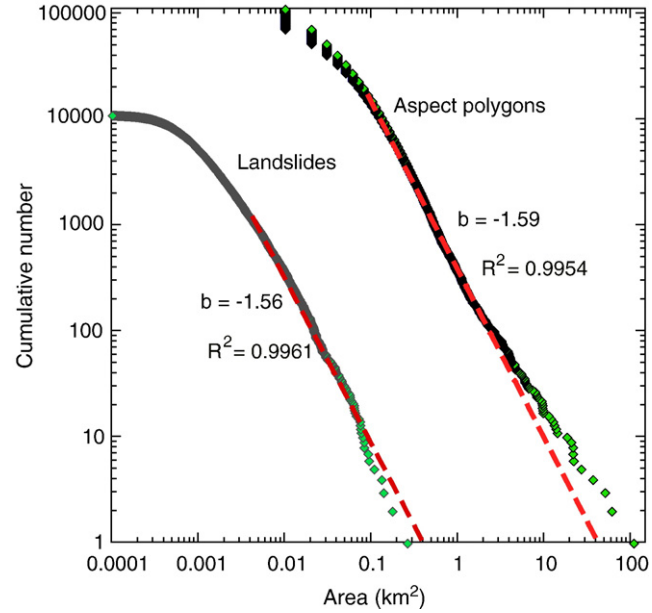

Fig. 12. Comparison between the cumulative area distribution of aspect polygons in the topography of the Northridge area (Fig. 9B) and the 1994 M6.7 Northridge earthquake landslide areas measured by Harp and Jibson (1995). Aspect polygon areas are discrete multiples of 0.01 km^2 due to the 100 m grid of the topography. Only the largest 8% of landslide areas (areas > 0.004 km^2) and the largest 7.5% of aspect polygon areas (areas > 0.12 km^2) were fit to achieve high degree of correlation with an inverse power law.

argue that landslides initiate simultaneously throughout the area affected by ground shaking. The slide products (debris flow, debris avalanche, turbidities, etc.) do not entrain significant volumes of new material during the runout. This hypothesis contradicts previous interpretations of landslides as a cascading avalanche, or self-organized critical process, where the landslide nucleates in one or few locations and propagates from there to the entire landslide region. Therefore, we argue that landslides should not be viewed together with earthquakes and fires (e.g., Malamud and Turcotte, 2006), as a process whose final size cannot be predicted at the onset of the disturbance.

The area distribution of submarine landslides along the Atlantic continental slope can be fit well by a lognormal distribution, whereas a cascading avalanche process is represented statistically by inverse power law distribution. Assuming that the size of failure area is related to earthquake magnitude via ground shaking and slope instability, we generated by Monte Carlo simulations area distributions, which fit the observed distribution and have lognormal distributions. However, we do not imply a genetic significance to lognormal distribution, but only that it represents a distribution with characteristic area with decreasing number of landslides of both larger and smaller areas.

We further show here and in a companion paper (ten Brink et al., 2009), that for a given earthquake magnitude, the predicted maximum failure area from slope stability analysis is comparable to the maximum observed area that encompasses all subaerial landslides from a single earthquake-triggered event. The many individual landslides within the observe land area can be perceived in the context of our hypothesis as many independent nucleating points triggered by a single event. Inverse power law, double Pareto, and Gamma distributions of these landslides sets within a single event may reflect the morphological characteristics of the affected area, and may not have intrinsic significance to the failure process. Thus, the study of landslide processes in the marine environment offers some advantages relative to land environments, in that small-scale morphology plays a lesser role in landslide distribution. Finally, the lack of double-couple earthquakes, generated by landslides, also argues against a propagation model for the failure interface. The hypothesis presented here, implies that the maximum area of landslides is generally predictable from the characteristics of the triggering event, however how much of that area will actually fail depends on local variations in slope angle, material strength, pore pressure, and the presence of pre-existing fractures.

Acknowledgements

Discussions with Andy Solow and helpful reviews by Eric Geist, Homa Lee, and Niels Hovius are gratefully acknowledged. Jeff Coe provided the digital elevation model used in Fig. 9 and Dave Mosher provided details about the 1929 Grand Banks landslide. Work was partially funded by U.S.-NRC grant N6480 *Physical study of tsunami sources*.

References

Bak, P., Tang, C., Wiesenfield, K., 1988. Self-organized criticality. Phys. Rev. 38, 336–374.
Bent, A.L., 1995. A complex double-couple source mechanism for the Ms 7.2 1929 Grand Banks earthquake. Bull. Seismol. Soc. Amer. 85, 1003–1020.
Boore, D.M., Joyner, W.B., 1997. Site amplifications for generic rock sites. Bull. Seismol. Soc. Amer. 87, 327–341.
Booth, J.S., O'Leary, D.W., 1991. A statistical overview of mass movement characteristics on the North American Atlantic outer continental margin. Mar. Geotechnol. 10, 10–18.
Bucknam, R.C., et al., 2001. Landslides triggered by Hurricane Mitch in Guatemala; inventory and discussion. OF 01-0443. U. S. Geological Survey, Reston.
Burroughs, S.M., Tebbens, S.F., 2001. Upper-truncated power laws in natural systems. Pure Appl. Geophys. 158, 741–757.
Campbell, K.W., 2003. Prediction of strong ground motion using the hybrid empirical method and its use in development of ground-motion (attenuation) relations in Eastern North America. Bull. Seismol. Soc. Amer. 93, 1012–1033.
Chaytor, J.D., ten Brink, U.S., Solow, A.R., Andrews, B.D., 2009. Size distribution of submarine landslides along the U.S. Atlantic margin and its implication to tsunami hazards. Mar. Geol. 264, 16–27.
Dai, F.C., Lee, C.F., 2001. Frequency–volume relation and prediction of rainfall-induced landslides. Eng. Geol. 59, 253–266.
Densmore, A.L., Ellis, M.A., Anderson, R.S., 1998. Landsliding and the evolution of normal-fault-bounded mountains. J. Geophys. Res. 103, 15,203–15,219.

Dunning, S.A., Mitchell, W.A., Petley, D.N., Rosser, N.J., Cox, N.J., 2007. Landslides predating and triggered by the 2005 Kashmir earthquake: rockfall to rock avalanches. Geophys. Res. Abstr. 9, 06376.
Dussauge, C., Grasso, J.-R., Helmstetter, A., 2003. Statistical analysis of rockfall volume distributions; implications for rockfall dynamics. J. Geophys. Res. 108, 2286. doi:10.1029/2001JB000650.
Frankel, A.D., et al., 1996. National seismic-hazard maps; documentation June 1996. OF 96-532. U. S. Geological Survey, Reston.
Geist, E.L., Lynett, P.J., Chaytor, J.D., 2009. Hydrodynamic modeling of tsunamis from the Currituck landslide. Mar. Geol. 264, 41–52.
Gutenberg, B., Richter, C.F., 1944. Frequency of earthquakes in California. Bull. Seismol. Soc. Amer. 34, 185–188.
Guthrie, R.H., Deadman, P.J., Cabrera, A.R., Evans, S.G., 2008. Exploring the magnitude–frequency distribution: a cellular automata model for landslides. Landslides 5, 151–159.
Guzzetti, F., Malamud, B.D., Turcotte, D.L., Reichenbach, P., 2002. Power-law correlations of landslide areas in central Italy. Earth Planet. Sci. Lett. 195, 169–183.
Hampton, M.A., Lee, H.J., Locat, J., 1996. Submarine landslides. Rev. Geophys. 34, 33–59.
Harbitz, C.B., 1992. Model simulations of tsunamis generated by the Storegga slides. Mar. Geol. 105, 1–21.
Harp, E.L., Jibson, R.W., 1995. Inventory of landslides triggered by the 1994 Northridge, California earthquake. OF 95-0213. U. S. Geological Survey, Reston.
Harp, E.L., Wilson, R.C., 1995. Shaking intensity thresholds for rock falls and slides; evidence from 1987 Whittier Narrows and Superstition Hills earthquake strong-motion records. Bull. Seismol. Soc. Amer. 85, 1739–1757.
Hergarten, S., 2003. Landslides, sandpiles, and self-organized criticality. Natural Hazards and Earth System Sciences 3, 505–514.
Hornbach, M.J., Lavier, L.L., Ruppel, C.D., 2007. Triggering mechanism and tsunamigenic potential of the Cape Fear slide complex. Geochm. Geophys. Geosyst. 8, Q12008. doi:10.1029/2007GC001722.
Hutton, E.W., Syvitski, J.P., 2004. Advances in the numerical modeling of sediment failure during the development of a continental margin. Mar. Geol. 23, 367–380.
Hynes-Griffin, M.E., Franklin, A.G., 1984. Rationalizing the seismic coefficient method. U.S. Army Engineer Waterways Experiment Station Misc. pap., GL-84-13, 21 pp.
Issler, D., De Blasio, F.V., Elverhoi, A., Bryn, P., Lien, R., 2005. Scaling behaviour of clay-rich submarine debris flows. Mar. Petrol. Geol. 22, 187–194.
Jibson, R.W., Harp, E.L., Michael, J.A., 1998. A method for producing digital probabilistic seismic landslide hazard maps: an example from the Los Angeles, California area, OF98-113. U.S. Geological Survey, Reston. 17 pp.
Kanamori, H., Given, J.W., 1982. Analysis of long-period seismic waves excited by the May 18, 1980, eruption of Mount St. Helens: a terrestrial monopole? J. Geophys. Res. 87, 5422–5432.
Katz, O., Aharonov, E., 2006. Landslides in a vibrating sand-box: what controls types of slope-failure and frequency magnitude relations? Earth Planet. Sci. Lett. 247, 280–294.
Keefer, D.K., 1984. Landslides caused by earthquakes. Geol. Soc. Amer. Bull. 95, 406–421.
Lee, H.J., 2009. Timing of occurrence of large submarine landslides on the Atlantic Ocean margin. Mar. Geol. 264, 53–64.
Lee, H.J., Locat, J., Dartnell, P., Minasian, D., Wong, F., 2000. A GIS-based regional analysis of the potential for shallow-seated submarine slope failure. Proc. 8th Int. sympos. on Landslides, Cardiff, Wales, June 26–30, pp. 917–922.
Locat, J., 2001. Instabilities along ocean margins: a geomorphological and geotechnical perspective. Mar. Petrol. Geol. 18, 503–512.
Locat, J., Lee, H.J., 2002. Submarine landslides: advances and challenges. Can. Geotech. J. 39, 193–212.
Locat, J., et al., 2009. Geomorphology, stability, and mobility of the Currituck slide. Mar. Geol. 264, 28–41.
Malamud, B.D., Turcotte, D.L., 2006. An inverse cascade explanation for the power-law frequency–area statistics of earthquakes, landslides and wildfires. In: Cello, G., Malamud, B.D. (Eds.), Fractal Analysis for Natural Hazards: Geological Society, London, Special Publications, pp. 1–9.
Malamud, B.D., Turcotte, D.L., Guzzetti, F., Reichenbach, P., 2004. Landslide inventories and their statistical properties. Earth Surf. Proc. Land. 29, 687–711.
Mazzotti, S., Adams, J., 2005. Rates and uncertainties on seismic moment and deformation in eastern Canada. J. Geophys. Res. 110, B09301. doi:10.1029/2004JB003510.
Meunier, P., Hovius, N., Haines, J.A., 2008. Topographic site effects and the location of earthquake induced landslides. Earth Planet. Sci. Lett. 275, 221–232.
Micallef, A., Berndt, C., Masson, D.G., Stow, D.A.V., 2008. Scale invariant characteristics of the Storegga Slide and implications for large-scale submarine mass movements. Mar. Geol. 247, 46–60.
Mosher, D.C., Piper, D.J.W., 2007. Analysis of multibeam seafloor imagery of the Laurentide Fan and the 1929 Grand Banks landslide area. In: Lykousis, V., Sakellariou, D., Locat, J. (Eds.), Submarine Mass Movements and Their Consequences. Springer, pp. 77–88.
Okal, E.A., 2003. T waves from the 1998 Papua New Guinea earthquake and its aftershocks: timing the tsunamigenic slump. Pure Appl. Geophys. 160, 1843–1863.
Okal, E.A., Synolakis, C.E., 2001. Comment on: "Origin of the 17 July 1998 Papua New Guinea Tsunami; earthquake or landslide?" by E.L. Geist. Seismol. Res. Lett. 72, 362–366.
Pelletier, J.D., Malamud, B.D., Blodgett, T.A., Turcotte, D.L., 1997. Scale-invariance of soil moisture variability and its implications for the frequency–size distribution of landslides. Eng. Geol. 48, 255–268.
Piper, D.J.W., Cochonat, P., Morrison, M.L., 1999. The sequence of events around the epicentre of the 1929 Grand Banks earthquake; initiation of debris flows and turbidity current inferred from sidescan sonar. Sedimentology 46, 79–97.
Pratson, L.F., Ryan, W.B.F., Mountain, G.S., Twichell, D.C., 1994. Submarine canyon initiation by downlslope-eroding sediment flows: evidence in late Cenozoic strata on the New Jersey continental slope. Geol. Soc. Am. Bull. 106, 395–412.
Rodriguez, C.E., Bommer, J.J., Chandler, R.J., 1999. Earthquake-induced landslides: 1980–1997. Soil Dyn. Earthqu. Eng. 18, 325–346.
Scholz, C.H., Cowie, P.A., 1990. Determination of total strain from faulting using slip measurements. Nature 346, 837–839.
Stark, C., Hovius, N., 2001. The characterization of landslide size distribution. Geophys. Res. Lett. 28, 1091–1094.
Stein, S., Wysession, M., 2003. An Introduction to Seismology, Earthquakes and. Earth Structure. Blackwell Publishing, Oxford. 498 pp.
Sugai, T., Ohmori, H., Hirano, M., 1994. Rock control on magnitude–frequency distribution of landslides. Trans. Jpn. Geomorph. Union 15, 233–251.
Talling, P.J., Amy, L.A., Wynn, R.B., 2007. New insight into the evolution of large-volume turbidity current: comparison of turbidite shape and previous modeling results. Sedimentology 54, 737–769.
Tavakoli, B., Pezeshk, S., 2005. Empirical-stochastic ground-motion prediction for eastern North America. Bull. Seismol. Soc. Amer. 95, 2283–2296.
ten Brink, U.S., Geist, E.L., Andrews, B.D., 2006a. Size distribution of submarine landslides and its implication to tsunami probability in Puerto Rico. Geophys. Res. Lett. 33, L11307. doi:10.1029/2006GL026125.
ten Brink, U.S., Geist, E.L., Lynett, P., Andrews, B., 2006b. Submarine slides north of Puerto Rico and their tsunami potential. In: Mercado, A., Liu, P.L.-F. (Eds.), Caribbean Tsunami Hazard. World Scientific, Singapore, pp. 67–90.
ten Brink, U.S., Lee, H.J., Geist, E.L., Twichell, D.C., 2009. Assessment of tsunami hazard to the U.S. East Coast using relationships between submarine landslides and earthquakes. Mar. Geol. 264, 65–73.
Tripsanas, E.K., Piper, D.J.W., Campbell, D.C., 2008. Evolution and depositional structure of earthquake-induced mass movements and gravity flows: Southwest Orphan Basin, Labrador Sea. Mar. Petrol. Geol. 25, 645–662.
Turcotte, D.L., Malamud, B.D., 2004. Landslides, forest fires, and earthquakes: examples of self-organized critical behaviour. Physica A 340, 580–589.
Twichell, D.C., Chaytor, J.D., ten Brink, U.S., Buczkowski, B., 2009. Geologic controls on the distribution of submarine landslides along the U.S. Atlantic Continental margin. Mar. Geol. 264, 4–15.
Wells, D.L., Coppersmith, K.J., 1994. New empirical relationships among magnitude, rupture length, rupture width, rupture area, and surface displacement. Bull. Seismol. Soc. Amer. 84, 974–1002.